AWARD NUMBER: W81XWH-14-1-0616

TITLE: Spinal Cord Injury-Induced Dysautonomia via Plasticity in Paravertebral Sympathetic Postganglionic

PRINCIPAL INVESTIGATOR: Shawn Hochman, PhD

CONTRACTING ORGANIZATION: Emory University
Atlanta, GA 30322

REPORT DATE: October 2017

TYPE OF REPORT: Annual

PREPARED FOR: U.S. Army Medical Research and Materiel Command
Fort Detrick, Maryland 21702-5012

REPORT DOCUMENTATION PAGE

Form Approved
OMB No. 0704-0188

1. REPORT DATE	2. REPORT TYPE	3. DATES COVERED
October 2017	Annual	30Sep2016 - 29Sep2017

4. TITLE AND SUBTITLE

Spinal Cord Injury-Induced Dysautonomia via Plasticity in Paravertebral Sympathetic Postganglionic

5a. CONTRACT NUMBER

5b. GRANT NUMBER

W81XWH-14-1-0616

5c. PROGRAM ELEMENT NUMBER

6. AUTHOR(S) **Shawn Hochman, PhD**

E-Mail:shochm2@emory.edu

5d. PROJECT NUMBER

5e. TASK NUMBER

5f. WORK UNIT NUMBER

7. PERFORMING ORGANIZATION NAME(S) AND ADDRESS(ES)

Emory University
599 Clifton Road, 4th Floor,
Atlanta, GA, 30322

8. PERFORMING ORGANIZATION REPORT NUMBER

9. SPONSORING / MONITORING AGENCY NAME(S) AND ADDRESS(ES)

U.S. Army Medical Research and Materiel Command
Fort Detrick, Maryland 21702-5012

10. SPONSOR/MONITOR'S ACRONYM(S)

11. SPONSOR/MONITOR'S REPORT NUMBER(S)

12. DISTRIBUTION / AVAILABILITY STATEMENT

Approved for Public Release; Distribution Unlimited

13. SUPPLEMENTARY NOTES

ABSTRACT Sympathetic postganglionic neurons (**SPNs**) located in sympathetic ganglia represent the final common sympathetic motor output. Even though SCI produces a profound plasticity in sympathetic autonomic function, the extent that SCI-induced dysautonomia is based on SPN changes within the thoracic paravertebral sympathetic chain is unknown. Given their strategic site in autonomic signaling to body, any plasticity is likely to be of high significance, yet there is a paucity of studies undoubtedly due to their near anatomical inaccessibility. We have solved the accessibility problem with a strategic methodological advance. We will determine the extent to which paravertebral SPNs are a nodal site for vasomotor dysfunction after SCI.

We will undertake physiological, pharmacological and optogenetic studies to examine network and cellular plasticity induced by SCI to answer the following two questions: (a) Does SCI lead to plasticity in synaptic interactions between preganglionics, SPNs and primary afferents? (b) Do SPNs become hyperresponsive to synaptic inputs after SCI?

14.

15. SUBJECT TERMS

Nothing listed

16. SECURITY CLASSIFICATION OF:			17. LIMITATION OF ABSTRACT	18. NUMBER OF PAGES	19a. NAME OF RESPONSIBLE PERSON
a. REPORT	b. ABSTRACT	c. THIS PAGE			USAMRMC
Unclassified	Unclassified	Unclassified	Unclassified	16	*19b.* **TELEPHONE NUMBER** *(include area code)*

Standard Form 298 (Rev. 8-98)

Contents

1. INTRODUCTION:

Sympathetic postganglionic neurons (**SPNs**) located in sympathetic ganglia represent the final common sympathetic motor output. Even though SCI produces a profound plasticity in sympathetic autonomic function, the extent that SCI-induced dysautonomia is based on SPN changes within the thoracic paravertebral sympathetic chain is unknown. Given their strategic site in autonomic signaling to body, any plasticity is likely to be of high significance, yet there is a paucity of studies undoubtedly due to their near anatomical inaccessibility. We have solved the accessibility problem with a strategic methodological advance. We will determine the extent to which paravertebral SPNs are a nodal site for vasomotor dysfunction after SCI.

We will undertake physiological, pharmacological and optogenetic studies to examine network and cellular plasticity induced by SCI to answer the following two questions: (a) Does SCI lead to plasticity in synaptic interactions between preganglionics, SPNs and primary afferents? (b) Do SPNs become hyperresponsive to synaptic inputs after SCI?

2. KEYWORDS:

spinal cord injury, sympathetic, autonomic, autonomic dysreflexia, spinal cord, electrophysiology, plasticity, paravertebral, postganglionic

3. ACCOMPLISHMENTS:

The PI is reminded that the recipient organization is required to obtain prior written approval from the awarding agency Grants Officer whenever there are significant changes in the project or its direction.

a. What were the major goals of the project?

1. *List the major goals of the project as stated in the approved SOW. If the application listed milestones/target dates for important activities or phases of the project identify these dates and show actual completion dates or the percentage of completion.*

Characterizing thoracic chain sympathetic postganglionics		
Major Task 1a: Convergence and divergence	**months**	**% completion/ Completion dates**
Subtask 1: Segment specific properties	1-6	75%
Subtask 2: Pharmacology	7-12	*75%*
Subtask 3: Breeding/crossing transgenic mice and spinalizations	1-36	18months behind target
Subtask 3: Establish intracellular recording techniques	3-18	100%
Major Task 1b: Convergence and divergence	**months**	
Subtask 1: Incorporation of optogenetic approaches for selective activation of neuron populations	12-18	100%
Milestone(s) Achieved: Understanding of synaptic organization in uninjured mice and ability to use optogenetics to selectively activate afferent and efferent fiber populations		
Intracellular recordings and optogenetics		
Major Task 2: Characterize mechanisms responsible for dysautonomia after spinal cord injury using intracellular recordings and optogenetics	**months**	**% completion/ Completion dates**
Subtask 1: Physiological plasticity in preganglionic-postganglionic interactions assessed using optogenetics	18-36	20%
Subtask 2: Physiological plasticity in afferent-postganglionic interactions assessed using optogenetics	18-36	0%
Subtask 3: Physiological plasticity in preganglionic-afferent interactions assessed using optogenetics	18-36	0%
Subtask 4: Intracellular recordings of synaptic and cellular plasticity in membrane properties; demonstration of membrane bistability	18-36	25%
Milestone(s) Achieved: Demonstration of important contribution of thoracic sympathetic chain to SCI-induced autonomic plasticity and forward insight into therapeutic interventions for future study		
Data analysis and publications		
Major Task 3: Data analysis and publications	**months**	**% completion/ Completion dates**
Subtask 1: Data analysis	6-36	55%
Subtask 2: Manuscript writing and submission	24-36	40%
Milestone(s) Achieved: Dissemination of scientific results.		

b. What was accomplished under these goals?

major activities; 2) specific objectives; 3) significant results or key outcomes, including major findings, developments, or conclusions (both positive and negative)

Accomplishments under specific sections are described below followed by an overall annual summary that synthesizes these accomplishments. Please refer to figures in the overall summary as needed.

1a.1: Segment specific properties

Methods/experiment: Mice are euthanized (.2mL 50% urethane) and thoracolumbar spinal column quickly removed. The vertebral column is cut longitudinally, both dorsally and ventrally, and spinal roots are severed to remove spinal cord. Remaining vertebral column and ribs are trimmed to include only the thoracic region*. The tissue is pinned down in a Sylgaard recording chamber and suction electrodes are positioned to stimulate various thoracic ventral roots and record from various thoracic ganglia.

Progress/results: In the annual progress report in 2016 we used extracellular recordings to show that there is a convergence onto individual ganglia. For example, stimulating T4-T11 ventral roots results in activity in the T11 ganglion. The studies involved electrical stimulation of ventral roots and we proposed to repeat these trials using a genetic approaches for optical stimulation of ventral roots. The advantage here is that recruitment is likely in size principle order and that use of ChAT::CHR2 ensures that axonal recruitment from ventral roots is exclusively recruiting preganglionic cholinergic neurons and not inadvertently activating primary afferents that we showed previously and as has been reported also project visceral afferents through some ventral roots in thoracic segments. We have just begun assessment using optogenetics including after spinal cord injury.

1a.2: Pharmacology

Methods/experiment: Dissected vertebral column described in the methods section above is pinned down in recording chamber with stimulating suction electrodes on various ventral roots and a recording electrode on thoracic ganglia. We have been testing for synaptic transmitter identity by applying glutamatergic, cholinergic, nitrergic, purinergic and adrenergic ionotropic receptor antagonists to the recording chamber.

Progress/results:

Extracellular Recordings. We have found evidence for a contribution from glutamatergic, nitrergic and cholinergic transmission in both ventral root and dorsal root evoked responses. Postganglionic transmission is thought to occur via nicotinic acetylcholine receptor subunits. We have conducted experiments with nAChR antagonists that act on different receptor subunits and have found reduction from baseline synaptic transmission. We have increase sample size in the previous year and we've also broadened our pharmacological approach to include assessment of neuromodulation by sympathomimetics that include octopamine as well as β-phenylethylamine.

Intracellular Recordings. Experiments continue to assess the effects of various channel blockers on intrinsic membrane currents and synaptic events in intracellular recordings from individual neurons (**Figure 1**).

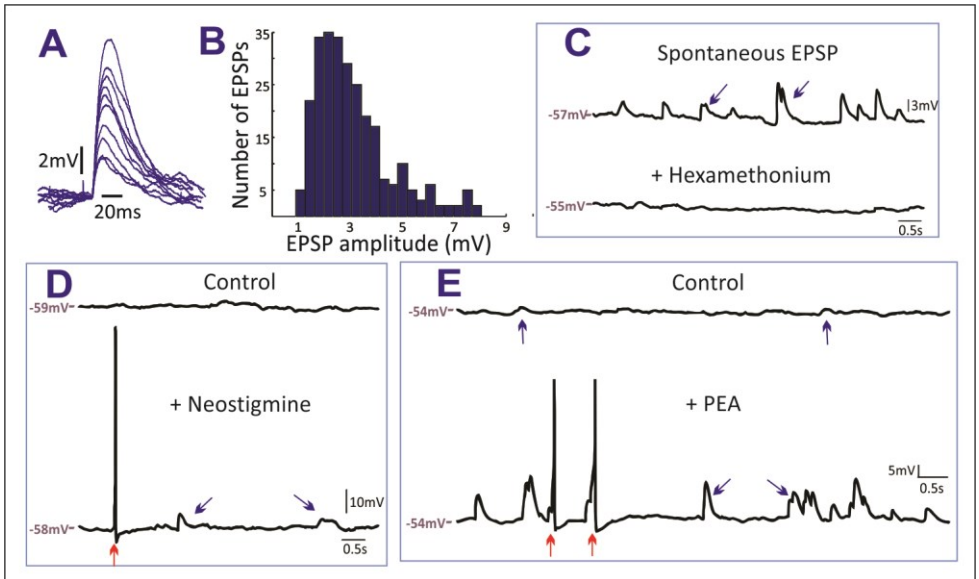

Figure 1. tSPN spontaneous EPSPs are cholinergic and modulated by PEA. A. Overlaid traces of captured EPSPs in one spontaneously active cell. **B**. Histogram of events showing that EPSP amplitudes occupy a continuous range from 1 to 8mV. C-D. Spontaneous EPSPs are cholinergic. They were blocked by 100uM hexamethonium (nAChR antagonist), and enhanced by 10uM neostigmine (acetylcholinesterase). E. 30uM PEA dramatically increased the amplitude and frequency of spontaneous EPSPs. Blue arrow: spontaneous EPSP. Red arrow: spontaneous EPSP triggered spike.

1a.3: Breeding/crossing transgenic mice and spinalizations
Methods/experiment: Standard animal husbandry
Progress/results: We currently have a healthy colony of ChAT-IRES-Cre::ChR2 mice available for performing in vitro optogenetic studies. We believe these mice will be more suitable than the BAC transgenics we previously used due to the more precise nature of their transgene insertion. These mice are used for all studies, with the exception of subtask 2.2. Subtask 2.2 will require the generation of Advillin::ChR2 mice to study afferent-postganglionic interactions. We are in possession of the requisite mouse strains, but have refrained from crossing them until other subtasks have neared completion.
As stated in the annual progress report in 2016, spinalizations are behind schedule. This has not changed. For example, in our last series of spinalizations with n=5, only one survived the requisite three week period we deemed necessary to examine plasticity at a time with known autonomic dysreflexia. Two animals were sacrificed early after spinalization (in the first week) due to health concerns. Two mice died from ruptured bladders due to manual expression even though individuals undertaking manual expression has significant experience, it appears that the bladder itself becomes more easily ruptured with manual expression pressures that previously were not sufficient to induce rupture. The difficulty of caring for injured mice compounded with the relatively low success rate of our intracellular recording technique has slowed progress in this area.
1a.4: Establish intracellular recording techniques
Methods/experiment: Starting with the preparation to isolate the thoracic chain and after ribs and vertebrae are trimmed (see 1a.1 methods, *) the entire tissue is incubated at 37°C in collagenase (and now dispase) for 1.5 hours. The tissue is then washed in physiological saline. Sympathetic chain is removed by severing rami and transferred to a recording chamber. Chain is pinned down in Sylgard, connective tissue is removed by scraping lightly with an insect pin, and recorded using standard patch clamp technique.
Progress/results: We now fully achieve acceptable recordings from most mice used in experiments, with recordings that can last > 1hour. These longer recordings are required to characterize convergent synaptic input properties and to study membrane current pharmacology. Progress overall has been steady, but still slower than we had hoped.

1b.1: Incorporation of optogenetic approaches for selective activation of neuron populations
Methods/experiment: We have developed a laser-diode based stimulator which allows for optical activation of preganglionic axons in ChAT::ChR2 mice. Light can be directed to illuminate ventral roots (primarily for extracellular recordings), interganglionic nerve, or thoracic ganglia.
Progress/results: Evoked synaptic response fatigues due to repeated stimulation, and takes seconds to recover. Details were described in the annual progress report for 2016. We have now begun to examine these evoked responses after SCI in the data has yet to be fully analyzed. Please refer back to last year's annual report for detailed observations.

2.1: Physiological plasticity in preganglionic-postganglionic interactions assessed using optogenetics
Methods/experiment: Methods described in 1b.1 are repeated in spinal cord injured mice.
Progress/results: Progress has been slow in this area. Tissue from injured mice appears to be more difficult to patch, i.e. high resistance seals are hard to achieve and recordings are "leaky." In light of this observation, we intend to stain the tissue for extracellular matrix components (collagen, chondroitin sulfate proteoglycans) to test the hypothesis that the extracellular matrix becomes denser after SCI. As stated previously, we have hired a new technician to help streamline the injury and recording process.

2.2: Physiological plasticity in afferent-postganglionic interactions assessed using optogenetics
Methods/experiment: &/ Progress/results: We have abandoned these experiments due to unanticipated difficulty in success rates and other experiments as well as difficulty in maintaining our Advillin-Cre breeding population.

2.3: Physiological plasticity in preganglionic-afferent interactions assessed using optogenetics
Methods/experiment: &/ Progress/results: We have abandoned these experiments due to unanticipated difficulty in success rates and other experiments as well as difficulty in maintaining our Advillin-Cre breeding population.

2.4: Intracellular recordings of synaptic and cellular plasticity in membrane properties; demonstration of membrane bistability
Methods/experiment:
Progress/results: SCI may induce greater frequency of spontaneous synaptic events. However, we currently have n=8, 3 of which are at early injury time, so this must be replicated before we can say this with confidence.

3.1: Data analysis
Methods/experiment: Data is analyzed in Clampfit, MATLAB, and/or Excel.

Progress/results: Basic cellular properties (input resistance, membrane capacitance, time constant, firing rate) have been analyzed. Analysis of synaptic properties are in progress.

3.2: Manuscript writing and submission
Methods/experiment: N/A
Progress/results: Manuscript writing is in progress. The abstract and methods and results sections are essentially complete. The results section is still in progress.

Further UPDATES.

(A) Characterization of cellular properties in adult mouse thoracic paravertebral ganglia.

By using whole-cell patch clamp recordings in intact thoracic ganglia, we have been able to record tSPNs in intact *ex vivo* thoracic ganglia to characterize their cellular and synaptic properties. We now have a trong dataset of 39 healthy cells is shown in Table 2 (mean values ± SD). Resting membrane potential, input resistance and membrane time constant (τ_m) were substantially higher than those reported in previous studies in the adult mouse (resting membrane potential is 10mV lower, input resistance is 9 times higher and τ_m is 13 times longer) (Jobling and Gibbins, 1999). Rheobase varied greatly between cells, but values were still approximately 10 times lower than those reported previously (Jobling and Gibbins, 1999). Threshold voltage was typically 18 mV higher than resting membrane potential, and action potentials displayed after-hyperpolarization. All neurons were capable of repetitive firing, in contrast to previous reports of only phasic firing with depolarizing current (Jobling and Gibbins, 1999). These differences are most likely due to the preservation of cell physiology with our whole-cell patch in contrast to the disruption of cell properties by impalement injury using sharp electrodes in previous studies. In our whole-cell patch, maximal firing rates observed in response to depolarizing current steps ranged from 14-17 spikes/sec. During intracellular depolarization, firing rate increased with increased current injection and cells sustained tonic firing. Spike frequency adaptation was also observed. All recorded properties are fully consistent with those reported recently with whole cell recordings in the rat superior cervical ganglia (Springer et al., 2015). We also observed a notable I_h current in 8 out of 13 cells. Its activation generally required hyperpolarization beyond -100mV and I_h current was more pronounced with greater hyperpolarization. With activation of I_h current, cells often displayed a post-inhibitory rebound spike, which may be a major factor contributing to oscillatory activity discussed below. We are also able to gauge the magnitude of A-type potassium currents (I_A). The current amplitude of I_A current amplitude following a hyperpolarization voltage step is comparable to reported study is comparable, but of much longer duration when compared to prior reports.

Table 2. *Summary of basic membrane properties*

Property	Mean	±	SD	*n*
Membrane properties				
Resting membrane potential, mV	-58.8	±	7.2 (39)	39
Input Resistance, MΩ	1072	±	553 (38)	38
Membrane time constant, ms	94.3	±	54.8 (38)	38
Capacitance, pF	89.2	±	26.8 (38)	38
Threshold				
Absolute voltage, mV	-41.2	±	7.1 (39)	39
Relative to V_{hold}, mV	26.0	±	7.7 (39)	39
Rheobase, pA	27.5	±	16.0 (39)	39
Action Potential				
Amplitude, mV	55.0	±	15.7 (39)	39
Peak, mV	13.8	±	18.2 (39)	39
Half-width, ms	4.6	±	1.1 (39)	39
Rise slope, mv/ms	47.3	±	24.2 (39)	39
Afterhyperpolarization				
Amplitude, mV	15.1	±	3.7 (26)	26
Half-decay, ms	80.8	±	34.9 (26)	26
Duration, ms	230	±	71 (26)	26
F-I slope				
Max., Hz/pA	0.126	±	0.033 (39)	39
Sustained, Hz/pA	0.075	±	0.025 (39)	39

While a full manuscript for submission on these membrane properties was expected to be submitted by June, additional observations and incorporation of additional modeling has extended the process and we now anticipate a submission date of December 2017. The current version of the manuscript is attached

Comparing cellular properties after SCI.
Changes in connectivity following SCI may involve anatomical changes in tSPNs themselves. First, in the sparsely-labeled TH::TdTomato healthy animal, we observed very few dendrites in adrenergic neurons in caudal compared to rostral thoracic paravertebral ganglia (annual report 2016). This lack of dendrites in caudal

Table 1. Mean area and diameter values (±SD)				
	SCI (N = 7)	**Naive (N = 5)**	**P-Value**	**Power**
Mean Area	298±45	374±61	**0.02**	0.70
Mean Diameter	20.9±1.3	23.5±1.8	**0.015**	0.75
Mean Numbers	194±77	271±127	**0.10**	0.34

ganglia is an important factor in considerations of tSPN excitability, including lack of persistent inward currents (**PICs**) and membrane bistability. In motoneurons, membrane bistability is associated with dendritic expression of PIC related voltage-gated channels. Thus anatomical changes such as increased dendritic arborization of tSPN will be consistent with the hypothesis that PICs emerge post-SCI.

Preliminary recordings suggest that I_A activation/inactivation dynamics may be lengthened after SCI (**Figure 2**). These preliminary studies of intrinsic cellular properties of unidentified tSPNs provide a demonstration of the power of whole patch recordings for discovery of tSPN physiology. With specific I targeting of NPY-positive vasoconstrictor tSPNs, I will be able to definitively determine intrinsic properties related to vasomotor function.

(B) Anatomical and synaptic plasticity after spinal cord injury.

Anatomical plasticity after spinal cord injury.

We have now compared counts and diameters of thoracic sympathetic postganglionic neurons from the T5 segment. Samples were in naïve controls (n=5) and mice having undergone spinal transection at thoracic level two (T2) three weeks prior (n=7). Adrenergic neurons were identified in whole ganglion immunohistochemical reaction for tyrosine hydroxylase (TH). Counts and size (area/diameter) of T5 neurons positive for TH were undertaken using Neurolucida software (MicroBrightField). We conducted t-tests with a significance level of α=0.05. We observed that after SCI, mean area and diameter of adrenergic neurons were statistically decreased (Table 1). We also compared average cell numbers, though there was a numerical 28% reduction in cell numbers after SCI, the observed significant variability and low sample size did not provide sufficient power to reliably determine statistical significance. Future plans are to increase our sample size as well as extend observations to other ganglia.

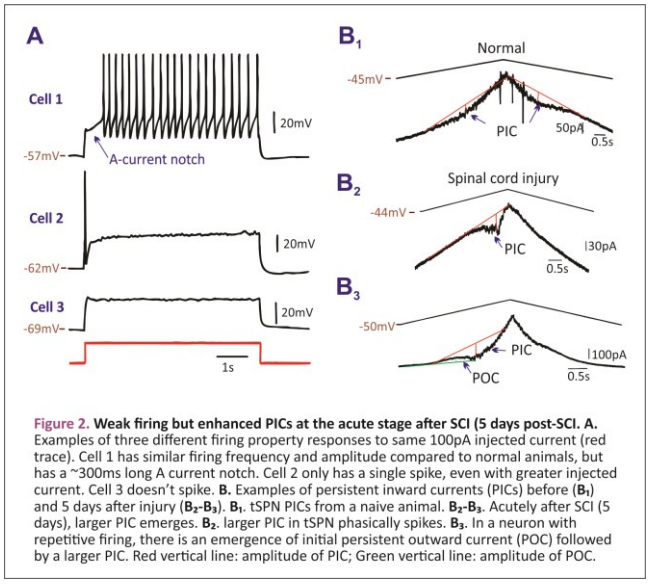

Figure 2. Weak firing but enhanced PICs at the acute stage after SCI (5 days post-SCI. A. Examples of three different firing property responses to same 100pA injected current (red trace). Cell 1 has similar firing frequency and amplitude compared to normal animals, but has a ~300ms long A current notch. Cell 2 only has a single spike, even with greater injected current. Cell 3 doesn't spike. **B.** Examples of persistent inward currents (PICs) before (B_1) and 5 days after injury (B_2-B_3). B_1. tSPN PICs from a naive animal. B_2-B_3. Acutely after SCI (5 days), larger PIC emerges. B_2. larger PIC in tSPN phasically spikes. B_3. In a neuron with repetitive firing, there is an emergence of initial persistent outward current (POC) followed by a larger PIC. Red vertical line: amplitude of PIC; Green vertical line: amplitude of POC.

Significant differences in cell area and diameter between SCI and naive T5 ganglia could be due to influence of sex rather than treatment. However, when we compared the average area and diameter of male versus females we saw no significant differences in mean areas or diameters. Within the constraints of our limited population size, we conclude that sex is not a factor.

Synaptic properties of paravertebral neurons.

The previous annual report (2016) provided details of our recordings of spontaneous and optogenetically evoked synaptic responses. This past year was associated with breeding issues that prevented us from undertaking various optogenetic stimulation experiments. Nonetheless we have had good success with increasing our success rate of whole cell recordings and this will enable a more complete assessment of ongoing spontaneous synaptic activity in the naïve preparation.

We have just begun to assemble data set of evoked responses in the spinal cord injured animals, but the data is too recent to provide quantitative analyses and is simply shown in figure that we believe is representative of observed differences (**Figure 3**).

We have also just begun to use an optogenetic approach to assess divergence of preganglionic axons arising from spinal segments onto individual thoracic chain ganglia onto individual tSPNs (*Fig X*). These results are also very recently obtained and preclude position of quantitative assessment at this stage.

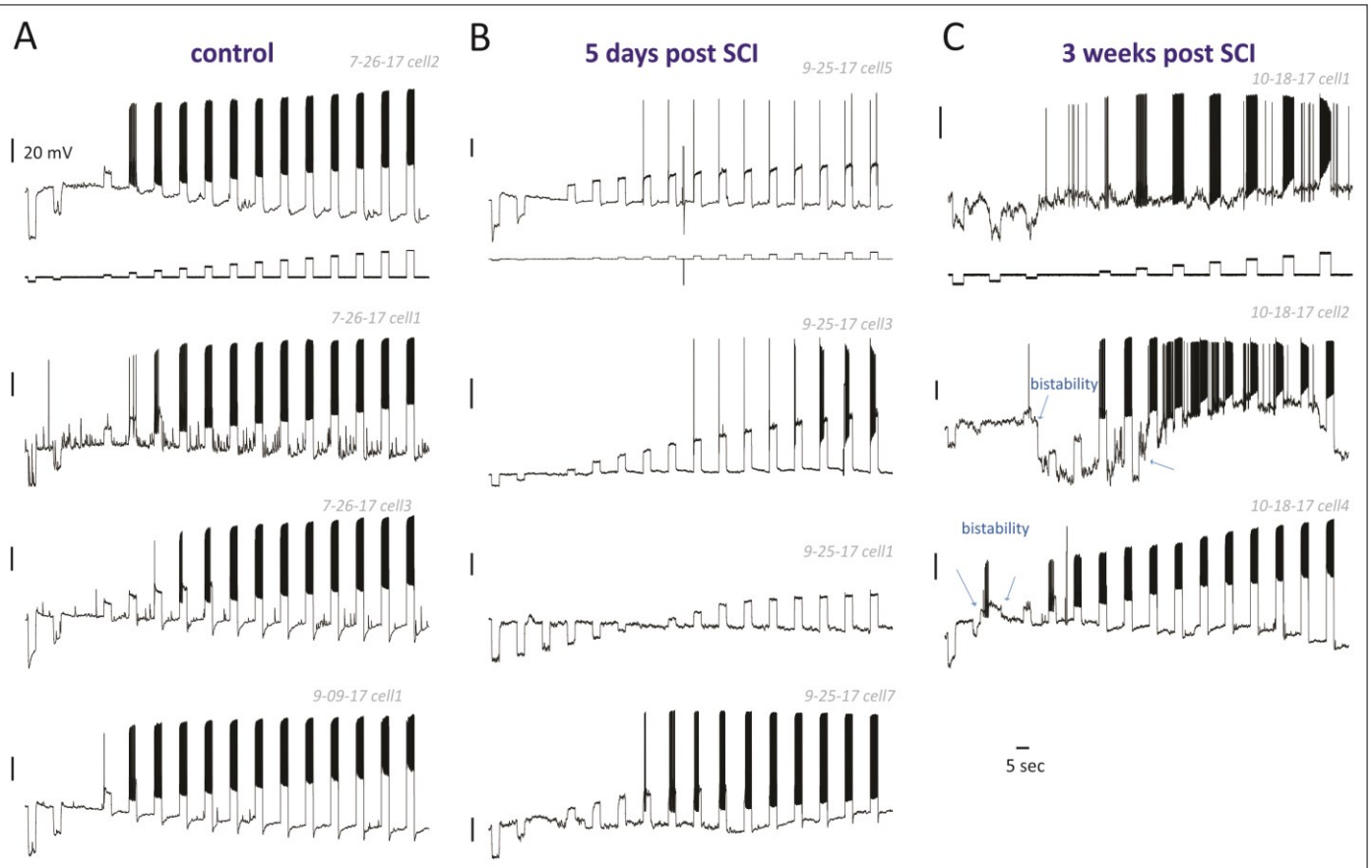

Figure 3. Comparison of firing properties in uninjured mice (A) and those having undergone T2 spinalization 5 days (B) or 3 weeks prior (C). A. Note that there is a sever reduction in excitability 5 days post-SCI (B) and that membrane potential instability including expression of shifts in membrane potential are notable 3 weeks post-SCI. Horizontal bar is 20 mV in all voltage recordings. Current step protocol is shown in upper row in all three panels.

4) other achievements.

Difficulty in obtaining recordings from spinal cord injured tissue.

We've had considerable difficulty in obtaining access to the cellular properties of these neurons after spinal cord injury. One possibility is that the injury leads to the generation of novel structural/cellular components that surround sympathetic ganglia. The working hard at trying to modify experimental approach and have begun to obtain success in the last month. This data has yet to be analyzed. Having said that recording quality has still been suboptimal and we have just ordered dispase as an additional protease to apply in conjunction with collagenase in an attempt to make the neuronal tissue more accessible.

We have found this to make an enormous difference and now have recordings from several neurons after spinal cord injury.

c. What opportunities for training and professional development has the project provided?

- *One individual was sent to a specialty meeting on spinal cord function in Marseille France to present his work and two individuals are being sent to the Annual Society for Neuroscience Meeting in San Diego this November.*

- *Three undergraduate students have worked on this project. Two of them I have worked on this model system in the last year, with one student undertaking a senior research project with poster present (attached).*

d. *Describe briefly what you plan to do during the next reporting period to accomplish the goals and objectives*.
   - *We have received a no-cost extension, we plan to stay consistent with the major tasks outlined in the charts except for Major Task 2, subtasks 2 and 3.*
   - *Regarding electrophysiology, emphasis will be on assessment of physiological plasticity*
   - *Regarding anatomical assessment, we will continue towards the changed emphasis on more overtly describing the previously implicit neuroanatomical assessment of injury-induced plasticity using immunolabeling approaches.*
   - *During this no-cost extension, a significant amount of time will be devoted to data analysis and manuscript writing.*

4. IMPACT:

- **What was the impact on the development of the principal discipline(s) of the project?**
  - *Nothing to Report*
- **What was the impact on other disciplines?**
  - *Led to a CRCNS application with a computational neuroscientist.*
  - *Led to a R01 application with a computational neuroscientist*
- **What was the impact on technology transfer?**
  - *Nothing to Report*
- **What was the impact on society beyond science and technology?**
  - *Nothing to Report.*

5. CHANGES/PROBLEMS:

Please see above. We have a no-cost extension to try and complete some of the major goals of the grant.

6. PRODUCTS:

Nothing to Report

Publications, conference papers, and presentations
Other publications, conference papers, and presentations. *Identify any other publications, conference papers and/or presentations not reported above. Specify the status of the publication as noted above. List presentations made during the last year (international, national, local societies, military meetings, etc.). Use an asterisk (*) if presentation produced a manuscript.*

1. M. L. MCKINNON, S. HOCHMAN. Patch clamp recordings of cellular and synaptic properties in adult mouse thoracic paravertebral ganglia. Soc. Neurosci. Abst. 42 (2016).
2. Halder, M.C., M.; MacDowell, C.; McKinnon, M.; Sawchuk,M.; Hochman,S. (2016). Anatomy of mouse thoracic sympathetic chain ganglia and electrophysiological assessment of their multisegmental preganglionic input. Paper presented at: Society for Neuroscience.
3. Choi MHH (2015) Anatomical survey of paravertebral sympathetic chain in adult mice. In: Department of Neuroscience and Behavioral Biology: Emory.

7. PARTICIPANTS & OTHER COLLABORATING ORGANIZATIONS

What individuals have worked on the project?

- *Mallika Halder – 25% effort – research specialist*
- *Michal McKinnon – 90% effort – graduate student*
- *Michael Sawchuk, - 50% effort - lab manager*
- *Yaqing Li – 33% effort - postdoctoral fellow*
- *Lucy Galvin – 10% effort - Senior undergraduate research project*

e. Has there been a change in the active other support of the PD/PI(s) or senior/key personnel since the last reporting period?

- *P.I. NIH R01. Recruitment principles and injury-induced plasticity in thoracic paravertebral sympathetic postganglionic neurons. 6/2017-6/2022, $1,250,000 direct.*
- *PI. Craig H Neilsen Foundation. Continuous sensor-based home-cage recordings for SCI research. 10/16-10/19, $600,000 total.*
- *Co-PI. [Garraway PI] Craig H Neilsen Foundation. Compromised Aδ-LTMRs function contributes to allodynia after SCI 8/16-8/18, $300,000 total.*

f. What other organizations were involved as partners?

- *Nothing to Report*

8. SPECIAL REPORTING REQUIREMENTS

9. APPENDICES:

g. paper in preparation

Passive and active properties of thoracic paravertebral neurons

Michael McKinnon, Kun Tian, Yaqing Li, Astrid Prinz Shawn Hochman

Abstract (250 words)

Paravertebral ganglia in the thoracic region of the sympathetic chain comprise the final common output of the sympathetic vasomotor system. Thoracic sympathetic postganglionic neurons (tSPNs) innervate vasculature and contribute to regulation of blood pressure. Despite the critical role tSPNs play in baroregulation, the electrophysiological function of thoracic paravertebral ganglia is poorly understood.

We obtained whole cell recordings to characterize electrophysiological properties of tSPNs. We found that basic membrane properties such as input resistance and time constant were much greater than values published in prior reports using sharp intracellular recordings. This implies that synaptic integration has a greater importance in driving sympathetic outflow than previously estimated. We found membrane resistivity to be the primary determinant of cell excitability. We also found that all cells fire repetitively for the duration of an injected current pulse, contrasting prior reports of predominantly phasic firing. Thus, tSPNs can maintain much higher firing rates than previously thought, which opens the door for neuromodulation to play a significant role. Our findings have implications for understanding how the vasomotor system goes awry following spinal cord injury induced dysautonomias such as autonomic dysreflexia.

Significance statement (120 words)

Thoracic sympathetic postganglionic neurons (tSPNs) represent the final common output of the sympathetic vasomotor system yet surprisingly little is known of their function. This study provides the first electrophysiological characterization of their cellular properties using whole cell recordings. We challenge the commonly held notion that paravertebral ganglia act as mere signal relays, and offer evidence of synaptic integration and neuromodulation.

Introduction (650 words)

Neurons that comprise the sympathetic nervous system are thought to share a common organization. Preganglionic neurons in the thoracolumbar spinal cord comprise the final common CNS output of the sympathetic nervous system. Preganglionics are cholinergic and, with few exceptions, synapse onto postganglionic neurons in sympathetic ganglia. Postganglionic neurons in turn innervate and control visceral organs. The majority of postganglionic neurons are adrenergic, while a few are cholinergic.

The paravertebral sympathetic chain (also known as the sympathetic trunk) comprises a group of interconnected sympathetic ganglia situated in the ventral side of the vertebral column. Whereas prevertebral sympathetic ganglia are typically associated with one or more visceral organs in a discrete location (celiac ganglion, superior/inferior mesenteric ganglion), paravertebral chain ganglia are associated with distributed organ systems such as vasculature, sweat glands, and piloerector muscles. As such, the sympathetic chain can be thought of as a distribution system for sympathetic activity that must span the body.

Ganglia in the thoracic region of the sympathetic chain comprise the primary postganglionic innervation of vasculature and contribute to blood pressure regulation. The electrical properties of sympathetic neurons have been studied in the superior cervical ganglion and to a lesser extent the stellate and lumbar ganglia, but to date only three studies have revealed electrophysiological properties of thoracic ganglia (Blackman & Purves, 1969a; P. Jobling & I. L. Gibbins, 1999; Lichtman, Purves, & Yip, 1980). As such, there is currently very little known about the electrical properties of ganglia within the thoracic chain. We undertook whole cell recordings to obtain the passive and active electrophysiological properties of tSPNs, and have generated a cellular computational model that supports ...

Surprisingly little is known about the thoracic segments of the sympathetic chain. We were guided by one primary question: what is the principle of recruitment of preganglionic axons? Two properties were characterized in postganglionic neurons: passive membrane properties, and active firing properties of postganglionic neurons.

Most thoracic paravertebral sympathetic postganglionic neurons (**tSPNs**) control vasomotor function in upper and middle extremities of the trunk. This includes vascular supply to integumentary, cardiorespiratory and digestive systems. Whereas prevertebral sympathetic ganglia are typically associated with one or more visceral organs in a discrete location, chain ganglia can be thought of as a distribution system for sympathetic activity that must span the body vasculature.

Unlike more rostral cervical and caudal lumbar chain ganglia (Bratton, Davies, Janig, & McAllen, 2010; Campanucci, Krishnaswamy, & Cooper, 2010; Percy & Krier, 1987; Rimmer & Horn, 2010; M. G. Springer, P. H. Kullmann, & J. P. Horn, 2015) (see also (I. L. Gibbins, Jobling, & Morris, 2003; Undem & Potenzieri, 2012; Wang, Holst, & Powley, 1995)), only 3 *in vitro* studies have revealed tSPN electrophysiological properties (Blackman & Purves, 1969a; P. Jobling & I. L. Gibbins, 1999; Lichtman et al., 1980). All used sharp microelectrode recordings with impalement injury, so there are still no reliable recordings of the cellular integrative properties underlying tSPN recruitment. Yet thoracic chain ganglia prominently control vasomotor actions to regulate vasculature in upper and middle extremities including bronchi, lungs, heart, esophagus, integumentary system and some viscera (Janig, 2006). *Why are there so few studies on tSPNs so clearly important in the regulation of cardiovascular function?* The answer is simple. They are deeply embedded and hidden within adherent fat attached adjacent to the ventral vertebral column and physically inaccessible for *in vivo* study. This void is glaring given that they may be the final arbiters of vasomotor control.

PNs are traditionally viewed as a homogeneous population driven by individual preganglionics that follow the 'n+1' rule (Karila & Horn, 2000; McLachlan, 2003). Computational models echo this viewpoint. For example, studies in bullfrog sympathetic ganglia (Karila & Horn, 2000; Wheeler, Kullmann, & Horn, 2004) assume sympathetic ganglia comprise a homogenous population of neurons with similar synaptic and firing properties. This implies that the entire ganglion can be understood by modeling a single ganglion cell. As outlined above, more recent work challenges this basic view (Bratton et al., 2010; M. G. Springer et al., 2015). Recordings from SPNs show marked heterogeneity in membrane properties (McKinnon, 2015; M. G. Springer et al., 2015)(*Fig 3*), cell body diameters vary several fold (*Fig 9*), neurons may or may not contain dendrites (*Fig 8*), synaptic input strengths occupy a large range (Blackman & Purves, 1969a)(*Fig 6*) and recruitment may follow the size principle (Cope & Pinter, 1995; Steinback, Salmanpour, Breskovic, Dujic, & Shoemaker, 2010).

First comprehensive understanding of recruitment principles in thoracic paravertebral sympathetic chain ganglia. ☺First computational model. This promises to deepen understanding and be an instructive guide for specific experimental testing. Insights derived from probing the network parameter space for putative neural bases of emergent dysfunction, could catalyze novelty in both experimental testing and in drug discovery-based therapeutic considerations.

A major function of sympathetic paravertebral chain ganglia neurons is to maintain vasomotor tone. While the functional properties of cervical and lumbosacral paravertebral ganglia neurons have been characterized, little is known about the functional properties of neurons within thoracic paravertebral ganglia. We developed an approach that allows for whole-cell patch clamp recordings in intact thoracic ganglia to characterize cellular and synaptic properties.

Threshold voltage was typically 10 mV higher than resting membrane potential, action potentials displayed after-hyperpolarization and some cells displayed post-inhibitory rebound. All neurons were capable of repetitive firing. Maximal firing rates observed in response to depolarizing current steps ranged from 14-17 spikes/sec. During intracellular depolarization, firing rate increases with increased current injection and cells sustain tonic firing. Spike frequency adaptation was also observed. All recorded properties are fully consistent with those reported recently with whole cell recordings in rat superior cervical ganglia (M. G. Springer et al., 2015). Strikingly, our recorded properties differ substantially from sharp electrode recordings obtained from adult mouse tSPNs (P. Jobling & I. L. Gibbins, 1999). Our recorded membrane resistance is 4.5 fold higher and τ_m is 7.5 fold longer than observed by Jobling and Gibbins (1999), and our neurons only fired tonically while theirs only fired phasically to depolarizing current pulses. Note that all of these differences are consistent with greater cell damage caused by sharp electrode penetration compared to patch clamp recordings. We therefore assume that our new whole cell recordings are closer to physiological reality.

Recruitment is determined by the minimum current required to evoke a single action potential (rheobase). There is limited understanding on the principles underlying recruitment of sympathetic postganglionic neurons. Regarding rheobase current the two most important measures influencing rheobase are voltage threshold and total cell membrane resistance (also called input resistance). If caudal thoracic chain postganglionic neurons are void of dendrites and approximate a spherical neuron, then the rheobase current is related to these parameters by Ohm's law $I_{RH}=V_{TH}/R_N$ with R_N being determined by cell surface area (A_N) and specific membrane resistivity (R_M). In somatic motoneurons, Gustafsson and Pinter (1984) found that motor neuron excitability (rheobase and voltage threshold) varied predominantly by variation in specific membrane resistivity (Gustafsson & Pinter, 1984a; Hochman & McCrea, 1994a).

From CRCNS

Sympathetic postganglionic neurons (**tSPNs**) represent the final common sympathetic motor output. Thoracic SPNs (**tSPNs**) located in paravertebral chain ganglia receive convergent input from preganglionic neurons, providing the dominant sympathetic control of vascular function in the trunk and upper extremities. Given their strategic nodal site in autonomic signaling to body, any plasticity in tSPNs is likely to be of high significance. Yet tSPNs are inaccessible for *in vivo* study, so operational principles are inferred from studies in cervical (Campanucci et al., 2010; Rimmer & Horn, 2010; M. G. Springer et al., 2015) and lumbar chain ganglia (Bratton et al., 2010; Percy & Krier, 1987). To date, only 3 *in vitro* studies have revealed tSPN electrophysiological properties (Blackman & Purves, 1969a; P. Jobling & I. L. Gibbins, 1999; Lichtman et al., 1980), and there are still no accurate recordings of their cellular integrative properties or underlying recruitment principles.

We undertook THE FIRST PHYSIOLOGICAL STUDIES ON CAUDAL THORACIC CHAIN GANGLIA IN THE ADULT MOUSE by developing an *ex vivo* preparation with intact segmental preganglionic and rostrocaudal interganglionic connections (M. a. H. Halder, S., 2015; M. S. Halder, M., and Hochman, S. , 2014). We also obtained the FIRST WHOLE CELL RECORDINGS OF tSPN synaptic and cellular properties (McKinnon, 2015). These data are a critical prerequisite to modeling studies, as observed synaptic integrative and firing properties are fundamentally different than previously observed with sharp electrodes due to impalement injury (P. Jobling & I. L. Gibbins, 1999; M. G. Springer et al., 2015). Our results already support tSPNs as overtly unique compared to SPNs characterized elsewhere.

tSPN Properties. A tSPN is recruited when sufficient depolarizing synaptic current is provided to initiate spiking. Do thoracic chain postganglionics vary in rheobase current? If so this differential excitability would be suggestive of a pre-synaptic organization that utilizes a recruitment strategy associated with differential excitability. In preliminary whole cell recordings, we have observed a range of rheobase and membrane resistance values that support a 10-fold population heterogeneity for recruitment. Moreover as there is a large range of cell body diameters (Figs 6&7), vasomotor control may follow a similar size principle of recruitment. Indeed, sympathetic postganglionics in human lumbar ganglia appear to have a range of conduction velocities and follow a size principle of recruitment (Steinback et al., 2010), supporting a relationship between recruitment order and axonal conduction velocity in the thoracic chain as well. (!) Cellular properties. As a guide we will use analogy to the known variation in cellular synaptic and conduction velocity properties in motor neurons consistent with a size principal organization (Cope & Pinter, 1995; Gustafsson & Pinter, 1984a, 1984c). We will plot rheobase against input resistance and membrane time constant to see if a similar relation exists for tSPNs. The resulting data will be used to create means and distributions of cellular properties that will inform the homogeneous and heterogeneous tSPN population models described above, respectively.

Methods

Immunohistochemistry

Two ChAT-eGFP mice (JAX:007902) were sacrificed by perfusion fixation at P91 and P101 respectively. They were anesthetized in an isofluorane chamber and injected with 40mg/kg urethane, intraperitoneally. The mice were then transcardially perfused through the ventricular catheter with saline and fixatives. The tissues were fixed in 4% paraformaldehyde overnight and transferred to a 15% sucrose solution and stored at 4°C. The tPSG (stellate-T13) were isolated and immersed in 15% sucrose for cryopreservation.

The isolated tissue was mounted on a frozen cryostat chuck using TissueTek® optimal cutting temperature compound. The chuck was left on dry ice for the tissue to freeze and placed in the cryostat at ~-21°C. The thickness of the sections was adjusted to 8 µm. Fisherbrand's superfrost/plus microscope slides were used to collect sectioned tissue. To avoid sampling errors, we counted SPNs on every section we obtained.

The slides were hydrated in phosphate buffered saline (PBS) for an hour and permeabilized with PBS containing 0.3% Triton X-100 (0.3% PBS-T) overnight. Subsequently, the sections were incubated for 2-3 days with the primary antibodies (Table 2). The preparations were then washed in 0.3% PBS-T (3X, 30 minutes), before incubating at 4°C with the secondary antibodies for 1.5 hours in room temperature (Table 3). The slides were left to dry after a final wash in PBS-T (20 minutes) and 50mM Tris-HCl (2X 20 minutes). They were then coverslipped with SlowFade® Gold antifade reagent with diamidino-2-phenylindole (DAPI).

The sections were analyzed under Olympus BX51. Neurolucida neuron tracing and counting software (MBF Bioscience) was used to trace the cell bodies (Figure 5B). The cell bodies were selected based on whether they were positive for ChAT and/or TH and whether their nuclei were present, as confirmed by DAPI staining to avoid redundant counting of the same cell body in different sections. Neurolucida Explorer was used to obtain the maximum and minimum feret values for each tracing. The cell diameter was calculated by averaging the two values.

Solutions

Unless otherwise noted, all recordings were made at room temperature in a bath of King's artificial cerebrospinal fluid (ACSF) containing (in mM) NaCl [127.99], KCl [1.90], MgSO4 *7H2O [1.30], CaCl2 *2H2O [2.40], KH2PO4 [1.20], glucose [9.99], and NaHCO3 [26.04]. ACSF pH adjusted to 7.4 after saturation with gas (95%O2, 5%CO2) at room temperature. Intracellular patch clamp solution contained (in mM) potassium gluconate [140.0], EGTA [11.0], HEPES [10], and CaCl2 [1.32] and was pH adjusted to 7.3 using KOH. Target osmolarity was less than 290mOsm. In most recordings (25/39 cells), support solution was added consisting of ATP [4.0] and GTP [1.0]. Liquid junction potential was calculated to be -9.8mV and empirically measured to be -13mV.

Dissection

Experiments were performed on adult (P37-379) C57BL/6 mice. All procedures were approved by the Emory University IACUC and conformed to the Guide for the Care and Use of Laboratory Animals. Mice were anesthetized with isoflurane and euthanized with urethane (0.2mL, 50% solution). Complete sedation was confirmed by lack of foot pinch and eye blink reflex. Skin on the back was removed. Two lateral incisions were made from the peritoneal cavity through the ribs and up to the neck. An incision was made through the lumbar spinal column and gently lifted upward. Viscera were carefully cut away leaving only spinal column, ribs, musculature, spinal cord, and sympathetic chain. A final cut through the cervical spinal cord frees the tissue from the mouse. This tissue is washed briefly in oxygenated ACSF to remove blood, and placed in a dissection chamber with ACSF. The preparation is pinned down dorsal side up. Fat, muscle, and connective tissue adherent to the vertebral column are removed, and a longitudinal incision is made through the midline of the dorsal vertebral column. The preparation is then flipped over and pinned ventral side up. We use the right thoracic chain, as it is more easily accessible. A careful incision is made just medial to the sympathetic chain to remove fat, connective tissue, and the descending aorta. This should expose the ventral surface of the spinal column. Now a second longitudinal cut is made on the contralateral side of the vertebral column, leaving the centrum for stability. The two halves of the spinal column are gently separated, pulling the spinal cord out and allowing exposed spinal roots to be severed. Once the spinal cord is removed, the ribs are trimmed short and the lumbar section is cut off just below the thirteenth rib. The entire prep is placed in a 1.5mL centrifuge tube and incubated in continually oxygenated ACSF containing collagenase (20mg Worthington type III per 1mL ACSF) for 1.5 hours. Following incubation, tissue is vortexed and washed with ACSF several times. The sympathetic chain is removed by severing rami, and is then pinned down into a clear Sylgaard recording dish, through which recirculating, oxygenated ACSF is perfused.

Whole cell patch clamp recordings

Whole-cell patch recordings were obtained from postganglionic cells. Cells were identified using an upright microscope (Olympus, BX51WI) affixed with a low-light camera (Olympus, OLY-150). Patch electrodes were pulled on a vertical puller (Narishige, PP-83) from 1.5mm outer diameter filamented, borosilicate glass capillaries (World Precision Instruments, stock # TW150F-4) for a resistance of 5-9MOhms. Signals were amplified using a MultiClamp 700A and digitized at 10 KHz using a Digidata 1322A and Clampex software (Axon Instruments).

Data analysis

All cellular properties were analyzed in Clampfit (Molecular Devices) or MATLAB (MathWorks). In current clamp mode, membrane voltage response to hyperpolarizing current steps of at least 1.5 seconds was fit to an exponential of the form [1] using the Levenberg-Marquardt algorithm built in to Clampfit. The tau term of the fit was used as the value of membrane time constant (τ_m) (Golowasch et al., 2009). R_N was estimated by dividing maximal voltage deflection (ΔV_f) by the injected current (I_{inj}) [2]. C_m was estimated by dividing τ_m by R_N [3].

[1] $\Delta V_f * \exp(-t/\tau_m) + C$, [2] $R_N = \Delta V_f / I_{inj}$, [3] $C_m = \tau_m / R_N$

Rheobase current was taken as the smallest long-duration (1.5 seconds or longer) positive current injection which elicited a single spike. In the case that an incremental increase in current elicited multiple spikes, rheobase was estimated to be the mean of the adjacent subthreshold and suprathreshold steps, e.g. if 30pA did not elicit any spikes but 40pA elicited several, the rheobase estimate would be 35pA.

Measured values related to action potential (AP) and post-spike afterhyperpolarization (AHP) characteristics were taken from single spikes elicited at rheobase current. Action potential threshold (threshold voltage) was taken to be the point at which the first derivative begins to increase at rheobase current injection (Platkiewicz & Brette, 2010). Action potential amplitude was defined as the difference between the peak voltage and threshold. AP half-width is the width of the spike at half AP amplitude. Afterhyperpolarization (AHP) amplitude was defined as the difference between peak negative voltage and steady-state voltage at rheobase current injection. AHP half-decay is the duration from peak AHP voltage to decay to half amplitude and AHP duration is the time between spike onset and return to baseline (Hochman & McCrea, 1994b).

Instantaneous firing rate (IFR) was taken as the inverse of the inter-spike interval. Maximal firing rate was the IFR for the first spike pair at the beginning of current onset. Sustained firing rate was the mean IFR for all subsequent spikes. Pulse duration was at least 1.5 seconds for all cells, and 3 seconds for the majority.

Liquid junction potential was calculated to be -9.8mV and empirically measured to be -13mV. All values of absolute voltage (RMP, Absolute threshold, peak) were corrected by -10mV.

Computational Modeling

<text>

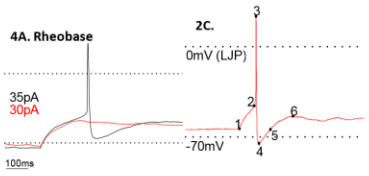

A: Schematic showing an example of a subthreshold (red, 30pA) and suprathreshold (black, 35pA) voltage trace. Rheobase for this cell was 35pA. C: Example trace from a neuron which fired a single spike at rheobase current injection. Numbered locations on the trace represent (1) the holding voltage: approximately -70mV, (2) threshold voltage: voltage at which the 1st derivative begins to increase significantly, (3) peak voltage: maximal voltage value, (4) AHP trough voltage: local minimum following peak, (5) AHP half-amplitude: mean of trough and steady-state voltage, and (6) steady-state voltage: voltage to which the membrane settles after spiking. Absolute voltage threshold is the value at (2). Relative voltage threshold is V_{2-1}. AP overshoot is the value at (3). AP amplitude is V_{3-2}. AP Halfwidth is the width of the AP halfway between (2) and (3). AP rise slope is the maximum slope between (2) and (3). AHP amplitude is V_{4-6}. AHP half-decay is t_{4-5}. AHP duration is t_{4-6}.

Results

Passive membrane properties

Whole cell patch clamp recordings were acquired from thoracic postganglionic neurons from the right thoracic ganglia with the majority of recordings coming from T5. The number of cells from ganglia T3 through T12 was 4,7,18,3,2,1,1,0,1, and 2, respectively. No significant differences were seen between ganglia so the data were pooled for population analysis. This does not rule out the possibility of subtle interganglionic variability, but we cannot say anything conclusively given the small sample size. In all, we recorded from 39 cells whose resting membrane potentials were more negative than -45mV, and thus deemed of sufficient quality. Basic cellular properties are summarized in Table 1. Resting membrane potential (RMP) was -59±7mV and ranged from -46 to -80mV (Fig. 2a). Input resistance (R_N) was 1072±553 MΩ and ranged from 237 to 2297MΩ. Membrane time constant (τ_m) was 94±55ms and ranged from 12.3 to 234ms. R_N and τ_m are, on average, an order of magnitude higher than values recorded using microelectrode recordings mouse (Phillip Jobling & Ian L. Gibbins, 1999) and guinea pig (Blackman & Purves, 1969b) thoracic ganglia. R_N was highly correlated with τ_m (R^2=0.69, n=38,$P<.00001$)(Fig. 2b), but not cell capacitance (R^2=.008, data not shown). This indicates that membrane resistivity, but not cell size, is responsible for the variability we see in resistance measures.

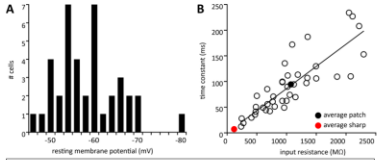

Figure 2: Passive membrane properties. A: Histogram showing distribution of resting membrane potential values. B: Input resistance is highly correlated with membrane time constant. Diagonal trendline indicates linear least-squares fit. Filled black circle represents population mean. Red filled circle, population mean from Jobling/Gibbins.

Property	Mean ± SD		
Membrane properties			
Resting membrane potential, mV	-58.8	±	7.2 (39)
Input Resistance, MΩ	1072	±	553 (38)
Membrane time constant, ms	94.3	±	54.8 (38)
Capacitance, pF	89.2	±	26.8 (38)
Threshold			
Absolute voltage, mV	-41.2	±	7.1 (39)
Relative to V_{rmp}, mV	26.0	±	7.7 (39)
Rheobase, pA	27.5	±	16.0 (39)
Action Potential			
Amplitude, mV	55.0	±	15.7 (39)
Peak, mV	13.8	±	18.2 (39)
Half-width, ms	4.6	±	1.1 (39)
Rise slope, mv/ms	47.3	±	24.2 (39)
Afterhyperpolarization			
Amplitude, mV	15.1	±	3.7 (26)
Half-decay, ms	80.8	±	34.9 (26)
Duration, ms	230	±	71 (26)
F-I slope			
Max., Hz/pA	0.126	±	0.033 (39)
Sustained, Hz/pA	0.075	±	0.025 (39)

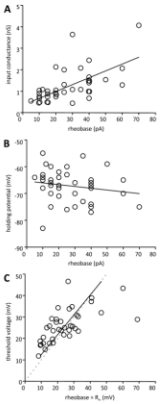

Figure 3: Rheobase. A: Rheobase was well correlated with input conductance. B: Rheobase was not correlated with holding potential. C: Rheobase "voltage" is approximately equal to threshold voltage.

Active membrane properties

Rheobase

The current required to depolarize a cell from its holding potential to firing threshold was examined in 39 cells by injecting long duration (1.5-3s) pulses through a patch electrode. In order to control for variable RMP, constant current was injected to hold cells at a standard holding potential of approximately -70mV prior to rheobase estimation. The minimum suprathreshold step required to elicit a single spike was taken as the rheobase. In cases where multiple spikes were elicited (n=12), the mean of the maximum subthreshold step and the minimum suprathreshold step was taken as the rheobase. Rheobase current varied in magnitude from 5 to 70pA with mean value of 27.5 pA (Table 1). The distribution of rheobase values can be seen on the abscissa in Fig. 4A. Rheobase values were much lower than those estimated previously in both mouse and guinea pig (Blackman & Purves, 1969b; Phillip Jobling & Ian L. Gibbins, 1999). Rheobase current was strongly correlated with input conductance, $g_{in}=R_{in}^{-1}$ (Fig. 3A, R^2=.37, n=38, P<.0001) and the inverse of time constant, τ_m^{-1} (R^2=.23, n=38, P<.003) and uncorrelated with capacitance (R^2=.01, n=38, P=.64). Despite best attempts to hold membrane potential steady, intrinsic variability in membrane voltage made this difficult to achieve in practice. We plotted actual holding voltage against rheobase to determine if this variability altered rheobase estimation. Rheobase was not correlated with membrane potential (Fig. 3B, R^2=.04, n=39, P=.23). Voltage threshold was assessed at rheobase current intensity. Assuming cell depolarization is governed by ohmic or non-rectifying processes, one would expect the product of rheobase and input resistance to predict the voltage threshold (Gustafsson & Pinter, 1984b). Indeed, the two values are well correlated (Fig. 3C, R^2=.41,n=38,P<.0001) and approximately equal, indicating the absence of rectifying currents around threshold voltage.

Post-spike afterhyperpolarization

Fast post-spike after-hyperpolarization (fAHP) amplitude and duration were assessed by measuring the time at half-decay and full fAHP duration. fAHPs were measured at rheobase current injection. fAHP amplitude and duration varied as a function of firing rate, so analysis of fAHP properties was limited to cells which fired a single spike at rheobase intensity (n=26). fAHP half-decay ranged from 28.6 to 152ms (80.8±34.9ms) and duration ranged from 109 to 363ms (230±71ms). Half-decay was very well correlated with duration (R^2=0.73, data not shown). We found half decay to be a more reliable measurement so further analysis focused on this parameter. fAHP half-decay was compared to basic membrane properties and rheobase (Fig. 5). fAHP half-decay was not correlated with R_{in} (R^2=.10, n=26, P=.12) or C_m (R^2=.06, n=26, P=.22), but slightly correlated with τ_m (R^2=.21, n=26, P=.02, Fig. 4A) and negatively correlated with rheobase (R^2=.27, n=26, P<.01, Fig. 4B). Previous studies have reported an inverse relationship between fAHP duration and firing rate in motoneurons ((Brownstone, Jordan, Kriellaars, Noga, & Shefchyk, 1992; Stauffer, McDonagh, Hornby, Reinking, & Stuart, 2007)). To determine if this relationship exists in postganglionic neurons, we plotted fAHP half-decay versus sustained firing rate at twice rheobase current injection. In cells which did not receive injection of twice rheobase (n=3), firing rate was estimated by interpolation or extrapolation. We found that there is indeed a very strong negative correlation between fAHP half-decay and firing rate at twice rheobase (R^2=.48, n=26, P<.0001, Fig. 4C)

Slow AHPs (sAHP) were also observed following strong depolarizing steps which elicited repetitive firing. Only cells displaying obvious sAHP were analyzed (n=30/39). Those cells excluded from analysis either did not display sAHP or the recording was too noisy to accurately measure sAHP parameters. sAHPs were measured at maximal current injection. The amplitude of sAHP increased with greater current injection, but the half-decay remained consistent within a cell for varied injected current. The half-decay of sAHPs and fAHPs were not correlated (R^2=.03, n=30). sAHPs had half-decay of 358±223ms, compared to the 81±35ms of the fAHP. Though longer duration AHPs have not been explicitly described in postganglionics, mAHPs (alternatively called mAHPs or sAHPs) have been attributed to activation of the M current (IM) and/or the calcium-dependent potassium current (IKCa) (Storm 1990, Yoshimura et. al. 1986, Sparnswick and Logan 1990, Inokuchi et. al. 1993). Further studies would be required to determine the relative contributions of these currents to the phenomena observed.

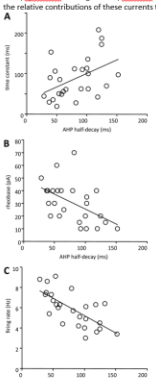

Figure 4: Afterhyperpolarization. A: AHP half-decay was correlated with τ_m (R^2=.21). B: AHP half-decay was negatively correlated with rheobase (R^2=.27). C: AHP half-decay was negatively correlated with firing rate at twice rheobase (R^2=.48)

Firing properties

Repetitive firing

Increasing current steps were delivered to assess repetitive firing properties from a holding potential of approximately -70mV. All cells (n=39) were capable of repetitive firing in response to sustained current injection. Fig. 5A shows an example of repetitive firing in response to progressively higher depolarizing current steps as well as a model neuron showing the same. Frequency-current relations (F-I) were obtained by plotting the maximal or sustained firing rate versus injected current magnitude. Fig. 5B and C show the maximal and sustained (respectively) F-I curves for all cells. Maximal instantaneous firing rate did not exceed 28 Hz, while sustained firing rate did not exceed 17 Hz for the highest steps given. Max F-I curves were approximately linear and sustained F-I curves were concave down. Slope for both max and sustained F-I curves was calculated as a measure of excitability. Mean values for max and sustained F-I slope are given in Table 1. Model neurons showed a similar max F-I curve (Fig. 5D). (Need to redo Fig. 5D, use max and sustained and systematically vary input resistance.) F-I slope was correlated with R_{in} (max: R^2=.24, n=38, p=.002, Fig. 5E; sustained: R^2=.19, n=38, p=.006). F-I slope was also negatively correlated with rheobase (max: R^2=.24, n=39, p=.002, Fig. 5F; sustained: R^2=.27, n=39, p<.001). No such relationship exits for time constant (max: R^2=.04; sustained R^2=.05) or capacitance (max: R^2=.01; sustained R^2=.07). AHP half-decay was significantly correlated with sustained F-I slope (R^2=.2084, n=26, p=.02) but not max F-I slope (R^2=.00, n=26, p=.96).

Spike rate adaptation

All cells displayed spike rate adaptation (SRA), or a decrease in firing rate over time (Fig. 6A,B). This feature was reproduced by the computational model (Fig. 6C,D). The difference between the initial firing rate and the sustained firing rate becomes more pronounced as injected current is increased (Fig. 6E). The ratio between the initial firing rate and the mean firing rate can be used as a measure of SRA. Recall that the sAHP has been attributed to IKCa and IM. Incidentally, both of these currents have also been implicated in SRA (Powers et. al. 1999, Benda and Tabak 2014, Miles at. al. 2005, Storm 1990). In order to examine the relationship between sAHP and SRA, we plotted the sAHP half-decay versus the SRA ratio (defined as the ratio between max firing rate and mean firing rate at the highest current injection) for 28 cells. We found that there was a statistically significant relationship (R^2=.27, n=28, p<.005), suggesting that there is indeed a relationship between SRA and sAHP (Fig. 6F).

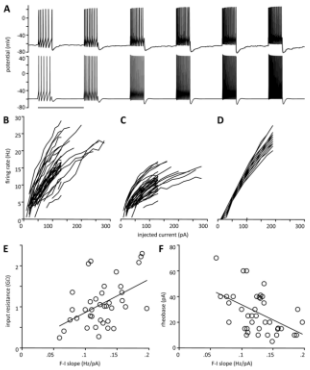

Figure 5: Repetitive firing. A: Top, representative trace showing repetitive firing in response to increasing current steps. Bottom, model neuron also showing repetitive firing. Injected current from left to right is 30, 50, 70, 90, 110, 130pA. Scale bar is 5 seconds. B: Maximal instantaneous firing rate is plotted versus injected current for all cells. C: Same as B with sustained firing rate. D: F-I curve from randomly chosen model neurons show a similar trajectory to the experimental data. E: Max. F-I slope is positively correlated with input resistance. F: Max. F-I slope is negatively correlated with Rheobase.

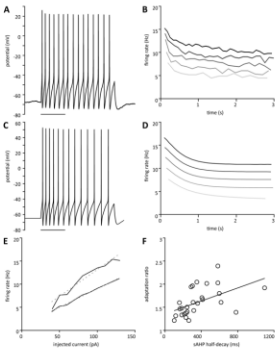

Figure 6: Spike rate adaptation. A: Representative trace showing cell response to 50pA current injection. Note that the inter-spike interval increases over time, corresponding to a decrease in instantaneous frequency. Scale bar is 1 second. B: Instantaneous frequency versus time for the same cell at (from bottom to top) 50, 70, 90, 110, 130 pA current injection C: Trace from a model cell shows spike rate adaptation for 50pA current injection. Scale bar is 1s. D: Instantaneous frequency versus time for the model cell in E. Injected currents were 50, 60, 70, 80, 90pA. E: F-I curve for max (top) and sustained (bottom) for the same cell. Dashed lines indicate linear regression. F: SRA ratio is positively correlated with sAHP half-decay (R^2=.27, n=28). Black line is the linear fit.

Subthreshold conductance

Anomalous rectification

During hyperpolarizing current injection, a depolarizing voltage "sag" was often observed. When present, a voltage sag was easily detected when cells were hyperpolarized beyond -100mV. The effect became more pronounced with greater hyperpolarization. In comparatively stable recordings, sag could occasionally be observed at less negative hyperpolarization (Fig. 7A). We found a voltage sag in 19 of 32 cells hyperpolarized to at least -100mV from a holding potential of -70mV. This phenomenon has been previously reported in tSPNs (Jobling/Gibbins) and other mammalian sympathetic neurons (Cassell et. al 1986) where it has been attributed to the anomalous rectifier, or H-current (I_h). I_h was implemented in the computational model and was found to reproduce the sag current (Fig. 7B). When cells held at -50mV, closer to firing threshold, cells often exhibited rebound firing upon release from hyperpolarization (Fig. 7C). Rebound firing has also been attributed to I_h (Pape 1996), but we found based on computational modelling that the primary driver of this phenomenon is Na+ channel de-inactivation during hyperpolarization (Kun: How do we know this? Why do we believe this is the case?) (Fig. 7D). This is further supported by the observation of rebound firing in the absence of voltage sag. The functional role of I_h in tSPNs remains unclear. It appears that I_h activation requires significant and prolonged hyperpolarization, yet there are no known inhibitory synapses within the sympathetic chain (McLachlan 2007). Prior reports also suggest that I_h contributes to the membrane potential at rest (Pape 1996) but we observe no relation between resting membrane potential and the presence of sag.

A-type potassium current

In response to depolarizing current steps, membrane voltage first follows an exponential time-course of depolarization with subsequent recruitment of voltage-gated conductances that alter the trajectory. When cells are depolarized from a holding potential of -70mV, observed recordings support recruitment of the voltage-gated sodium conductance first, detected as a positive deviation from the passive exponential trajectory. However, when cells are depolarized from a more negative holding potential of -90mV, the membrane trajectory has reduced slope and occasionally overt membrane hyperpolarization, both of which are consistent with activation of a voltage-gated K+ conductance. This was observed in 25 of 39 cells. The observed reduced slope in membrane led to a delay in the first action potential in a train (Fig. 7E). This phenomenon has been described previously in sympathetic neurons (Jobling/Gibbins) and is likely due to de-inactivation of A-type potassium current (I_A) at hyperpolarized voltages (Rush & Rinzel, 1995). To test this, we held a model neuron at two different holding potentials and found that the change in trajectory is indeed due to de-inactivation of A-current (Fig. 7F).

Also cite Connor and Stevens 1971
IA studied in rat SCG (Belluzzi et. al. 1985, Belluzzi and Sacchi 1986)

M-current in bullfrog (Brown and Adams 1980)

Rebound spiking may be due to Na de-inactivation, H-current helps a little but primarily Na de-inact.

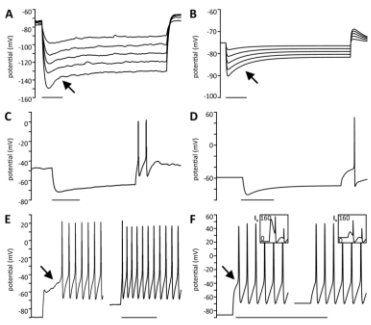

Figure 7: Subthreshold conductance. A: Voltage "sag," indicated by arrow, upon hyperpolarization beyond -90mV in a cell held at -70mV. Note that the effect becomes more pronounced with greater hyperpolarization. C: Hyperpolarizing trace from a different cell held at -50mV showing rebound spiking associated with voltage sag. E: A cell depolarized from -90 mV(LJP) exhibits a characteristic notch accompanied by a delay in spiking (left trace). The same cell depolarized from -70mV does not have a notch (right trace). F: Model neuron showing pre-spike inflection for hyperpolarized trace. Insets: I_h magnitude in pA at onset of current injection. Horizontal axis 150ms, vertical axis 0 to 160pA. Scale bars represent 500ms for all panels.

Cell firing type classification

We noted variability in spike height of the initial spike compared to subsequent spikes in a spike train during repetitive firing. Neurons were divided into three categories based on the peak voltage of the initial spike in a spike train compared to the peak voltage of subsequent spikes. Of the 39 neurons examined, the initial spike was slightly shorter than subsequent spikes in 22 cells (type 1), and substantially higher in 13 cells (type 2) (Fig. 8A). In type 1 and 2 cells, this phenomenon became more pronounced with greater current injection. In 4 cells, both firing patterns were observed, with type 1 characteristics at lower current steps giving way to type 2 characteristics at higher current steps (type 3). The difference between the initial spike peak voltage and the mean spike peak voltage was plotted for all cells as a function of calculated change in membrane voltage (injected current x R_{in}) (Fig. 8B). These differences did not appear to be associated with any basic membrane properties (R_{in}, τ_m, C_m, RMP), but a one-way ANOVA indicated that cell types differed significantly in terms of maximal rise slope (Fig. 8C), peak value (Fig. 8D), spike amplitude, and spike half-width. A summary of statistical measures is given in Table 2. Only parameters related to AP shape showed any significant difference between groups, and all such parameters showed significant differences between type 1 and type 2 cells.

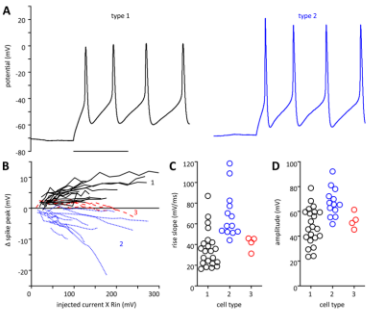

Figure 8: Cell type classification. A: Example traces from a type 1 (left, black) and type 2 (right, blue) cell. Scale bar 200ms. B: Population of cells showing a variety of firing types. The difference in the initial spike peak versus the mean of all subsequent spike peaks is plotted versus the product of injected current and input resistance for all cells (n=39). Type 1 cells with a positive change in spike peak are shown in solid black line; Type 2 cells with a negative change in spike peak are shown in dotted blue line; Type 3 cells which convert from type 1 to type 2 dynamics as injected current is increased are shown in dashed red line. C: Maximal rise slope for all three cell types. Type 2 cells have a significantly higher rate of depolarization than type 1 and 3 (P=.001; P=.04 respectively). D: Peak value for the initial spike at rheobase current injection. Type 2 cells have significantly higher peak values than type 1 but not type 3 (P=.001; P=.09 respectively).

Table 2. Comparison of basic properties of neuron subtypes

	Type 1	Type 2	Type 3	
Membrane properties				
RMP, mV	-58.7 ± 7.8 (22)	-57.5 ± 6.2 (13)	-63.0 ± 6.8 (4)	$F_{2,36}$=.87 P=0.43
R_{in}, MΩ	1070 ± 603 (22)	1006 ± 525 (12)	1285 ± 381 (4)	$F_{2,36}$=0.37 P=0.69
τ, ms	100.0 ± 59.7 (22)	85.0 ± 55.3 (12)	90.8 ± 16.5 (4)	$F_{2,36}$=0.29 P=0.75
C_m, pF	95.1 ± 28.9 (22)	83.7 ± 23.7 (12)	73.0 ± 15.4 (4)	$F_{2,36}$=1.6 P=0.23
Threshold				
Absolute, mV	-42.2 ± 7.1 (22)	-38.9 ± 7.7 (13)	-43.2 ± 4.2 (4)	$F_{2,36}$=1.0 P=0.36
Relative, mV	26.7 ± 8.0 (22)	25.5 ± 7.1 (13)	23.6 ± 9.1 (4)	$F_{2,36}$=0.31 P=0.74
Rheobase, pA	30.1 ± 17.3 (22)	26.2 ± 13.3 (13)	17.5 ± 15.5 (4)	$F_{2,36}$=1.1 P=0.33
Action potential				
Amplitude, mV	48.1 ± 14.8* (22)	67.3 ± 11.6[b] (13)	52.6 ± 6.6 (4)	$F_{2,36}$=8.5 P<0.001
Peak, mV	6.0 ± 18.0* (22)	28.3 ± 10.4[b] (13)	9.4 ± 9.3 (4)	$F_{2,36}$=9.0 P<0.001
Half-width, ms	5.1 ± 1.1* (22)	3.8 ± 0.7[b] (13)	4.4 ± 0.5 (4)	$F_{2,36}$=8.5 P<0.001
Rise slope, mV/ms	35.9 ± 18.2* (22)	68.7 ± 22.8[b] (13)	41.0 ± 6.8* (4)	$F_{2,36}$=12.1 P<0.0001
AHP				
Amplitude, mV	-14.3 ± 3.1 (15)	-16.8 ± 4.5 (9)	-13.3 ± 3.2 (2)	$F_{2,26}$=1.5 P=0.24
Half-decay, ms	89.1 ± 28.3 (15)	65.9 ± 38.3 (9)	85.8 ± 66.3 (2)	$F_{2,26}$=1.3 P=0.29
Duration, ms	252 ± 61 (15)	205 ± 76 (9)	181 ± 101 (2)	$F_{2,26}$=1.9 P=0.18

Values given as mean ± SD with number of observations in parentheses. RMP, resting membrane potential; R_{in}, input resistance; τ, membrane time constant; C_m, membrane capacitance; AHP, afterhyperpolarization. *,[b]Statistically different groups as determined by one-way ANOVA and Tukey's post hoc test.

Discussion (1500 words)

Include section talking about significance of rin, tau, rheobase being lower as a result of recording methodology.

Basic properties:

RMP is ~10mV more depolarized compared to Jobling/Gibbins

Need to talk about leak conductance in discussion and consequence on firing properties and cite Staley & Mody[Staley, 1992 #24456] paper comparison as well as Horn (M. G. Springer, P. H. M. Kullmann, & J. P. Horn, 2015).

Subthreshold conductances

Approximately half of cells exhibited a sag conductance when hyperpolarized below resting potential. This likely underlies the occasional rebound spiking observed upon release from hyperpolarization. While presence of H-current is interesting, the physiological relevance is less clear. It has long been known that there are no inhibitory synapses in the sympathetic chain (source). However, the existence of inhibitory neuromodulation which may activate Ih cannot be ruled out.

A-type potassium current (Ia) appears to play a significant role modulating the excitability of tSPNs. As the maximal Ia conductance increases, greater current is required to reach threshold. In addition, Ia increases AHP duration so cells with a high maximal Ia conductance are able to maintain lower continuous firing frequencies than similar cells with lower abundance of Ia.

The most abundant A-type potassium channels in sympathetic ganglia are Kv3.4, Kv4.1, and Kv4.2 (Dixon/McKinnon 1996).

A-current is also associated with a delay in spiking following a release from hyperpolarization (Fig. 4b). When cells are held at hyperpolarized potentials, Ia becomes significantly de-inactivated compared to rest. Upon release from hyperpolarization to a level which would elicit continuous firing, we observe a delay in the initial spike. According to Rush/Rinzel, this delay in spiking is strongly associated with the inactivation time constant of Ia.

The presence of A-type potassium current was also revealed by hyperpolarizing cells beyond resting potential. The inhibitory role of A-current is responsible for lengthening AHPs and lowering the minimum sustained firing rate (source). A-current can also shift the threshold for repetitive firing (Rush 1995).

All cells fired repetitively. This contrasts with previous studies with sharp electrodes, which report phasic firing in thoracic mouse neurons (Ian Lewis Gibbins, Jobling, Messenger, Teo, & Morris, 2000).

Maximal rise slope of action potential has been used as a proxy for sodium channel availability inactivation (Miles, Dai, & Brownstone, 2005). We plotted ... and also see a correlation between instantaneous firing rate and action potential rise slope (Fig. 5). In addition, (Powers, Sawczuk, Musick, & Binder, 1999) studied Initial adaptation in hypoglossal motoneurons and determined AHP summation to be the primary driver. To replicate this, we plotted spike frequency versus AHP amplitude and found ....

We conclude that both are involved (assuming plot shows this to be true) ...

In motoneurons, there are three phases of SRA: initial (first spike, 100ms), early (up to a few seconds), and late (up to 60 seconds) (Powers et al., 1999). Postganglionic neurons appear to exhibit initial and early-phase adaptation (Fig x). Late phase adaptation was not examined in the present study.

[Discussion] Previous studies have implicated sodium channel inactivation (Miles et al., 2005) and AHP summation (Powers et al., 1999)as possible mechanisms for SRA. Powers studied Initial adaptation in hypoglossal motoneurons and determined AHP summation to be the primary driver. Brownstone et. al. studied the mechanism of early-phase SRA more extensively in motoneurons and determined that the early-phase of SRA is governed by decreased availability of active sodium channels.

We further tested this hypothesis by removing the s term of gNa from our computational model and showed that no SRA was observed [was going to ask Kun to do].

This suggests that early phase SRA is likely due to sodium channel inactivation.

Multiple factors may contribute to SRA. According to our model, adjusting x and y reproduces SRA in model neurons.

Fig. 5e Spike rate adaptation

Taken together, a picture begins to emerge in which a population of cells resides on a spectrum of excitability. On one end of this spectrum are cells with low excitability. These cells have low input resistance and short time constants, which results in higher rheobase and a shallower F-I slope. On the other extreme are higher resistance cells with longer time constants, lower rheobase, and steeper F-I slope.

Choline blocks BKCa channels in mouse celiac ganglia (Delmas and Gola, 1995). KCa channels are likely responsible for the hyperpolarization following repetitive firing, a phenomenon well characterized in hippocampal cells (

The medium to long duration afterhyperpolarization has not to our knowledge been studied in sympathetic postganglionics. However, mechanisms underlying similar AHPs present in hippocampal neurons have been thoroughly worked out. AHPs of intermediate duration following repetitive firing are likely due to a combination of IM or the IKCa (Storm 1990), therein termed mAHP. In preganglionic neurons the phenomenon was similarly attributed to IKCa in cat (Yoshimura et. al. 1986, Inokuchi et. al 1993) and neonatal rat (Spanswick and Logan 1990), termed sAHP in both studies.

References

Blackman, J. G., & Purves, R. D. (1969a). Intracellular recordings from ganglia of the thoracic sympathetic chain of the guinea-pig. *J Physiol., 203*(1), 173-198.

Blackman, J. G., & Purves, R. D. (1969b). Intracellular recordings from ganglia of the thoracic sympathetic chain of the guinea-pig. *The Journal of Physiology, 203*, 173–198.

Bratton, B., Davies, P., Janig, W., & McAllen, R. (2010). Ganglionic transmission in a vasomotor pathway studied in vivo. *J Physiol., 588*(Pt 9), 1647-1659. doi: 1610.1113/jphysiol.2009.185025. Epub 182010 Mar 185022.

Brownstone, R. M., Jordan, L. M., Kriellaars, D. J., Noga, B. R., & Shefchyk, S. J. (1992). On the regulation of repetitive firing in lumbar motoneurones during fictive locomotion in the cat. *Exp Brain Res, 90*(3), 441-455.

Campanucci, V., Krishnaswamy, A., & Cooper, E. (2010). Diabetes depresses synaptic transmission in sympathetic ganglia by inactivating nAChRs through a conserved intracellular cysteine residue. *Neuron., 66*(6), 827-834. doi: 810.1016/j.neuron.2010.1006.1010.

Cope, T. C., & Pinter, M. J. (1995). The size principle: Still working after all these years. *News in Physiological Sciences, 10*, 280-286.

Gibbins, I. L., Jobling, P., Messenger, J. P., Teo, E. H., & Morris, J. L. (2000). Neuronal morphology and the synaptic organisation of sympathetic ganglia. *Journal of the Autonomic Nervous System, 81*, 104–109.

Gibbins, I. L., Jobling, P., & Morris, J. L. (2003). Functional organization of peripheral vasomotor pathways. *Acta Physiol Scand, 177*(3), 237-245. doi:10.1046/j.1365-201X.2003.01079.x

Golowasch, J., Thomas, G., Taylor, A. L., Patel, A., Pineda, A., Khalil, C., & Nadim, F. (2009). Membrane capacitance measurements revisited: dependence of capacitance value on measurement method in nonisopotential neurons. *J Neurophysiol, 102*(4), 2161-2175. doi:10.1152/jn.00160.2009

Gustafsson, B., & Pinter, M. J. (1984a). An investigation of threshold properties among cat spinal alpha-motoneurones. *J Physiol, 357*, 453-483.

Gustafsson, B., & Pinter, M. J. (1984b). An investigation of threshold properties among cat spinal alpha-motoneurones. *The Journal of Physiology, 357*, 453.

Gustafsson, B., & Pinter, M. J. (1984c). Relations among passive electrical properties of lumbar alpha-motoneurones of the cat. *J Physiol, 356*, 401-431.

Halder, M. a. H., S. (2015). *Early insight into emergence of spontaneous synchronous oscillatory activity in isolated thoracic chain ganglia after SCI.* Paper presented at the 8th SFN Satellite Symposium on Motor Systems, Chicago.

Halder, M. S., M., and Hochman, S. . (2014). *Sympathetic preganglionic and afferent stimulation-evoked responses in paravertebral thoracic chain ganglia.* Paper presented at the Soc. Neurosci. Abst. 40.

Hochman, S., & McCrea, D. A. (1994a). Effects of chronic spinalization on ankle extensor motoneurons. II. Motoneuron electrical properties. *J Neurophysiol, 71*(4), 1468-1479.

Hochman, S., & McCrea, D. A. (1994b). Effects of chronic spinalization on ankle extensor motoneurons. II. Motoneuron electrical properties. *Journal of Neurophysiology, 71*, 1468–1479.

Janig, W. (2006). *The Integrative Action of the Autonomic Nervous System*: Cambridge University Press.

Jobling, P., & Gibbins, I. L. (1999). Electrophysiological and morphological diversity of mouse sympathetic neurons. *J Neurophysiol, 82*(5), 2747-2764.

Jobling, P., & Gibbins, I. L. (1999). Electrophysiological and morphological diversity of mouse sympathetic neurons. *Journal of Neurophysiology, 82*, 2747–2764.

Karila, P., & Horn, J. P. (2000). Secondary nicotinic synapses on sympathetic B neurons and their putative role in ganglionic amplification of activity. *Journal of Neuroscience, 20*(3), 908-918.

Lichtman, J. W., Purves, D., & Yip, J. W. (1980). Innervation of sympathetic neurones in the guinea-pig thoracic chain. *J Physiol., 298*, 285-299.

McKinnon, M. C., M.H.; Hochman, S. . (2015). *Characterization of cellular and synaptic properties in adult mouse thoracic paravertebral ganglia.* Paper presented at the 8th SFN Satellite Symposium on Motor Systems.

McLachlan, E. M. (2003). Transmission of signals through sympathetic ganglia--modulation, integration or simply distribution? *Acta Physiol Scand, 177*(3), 227-235. doi:10.1046/j.1365-201X.2003.01075.x

Miles, G. B., Dai, Y., & Brownstone, R. M. (2005). Mechanisms underlying the early phase of spike frequency adaptation in mouse spinal motoneurones: Mechanisms underlying SFA in spinal motoneurones. *The Journal of Physiology, 566*, 519-532. doi:10.1113/jphysiol.2005.086033

Pape, H.-C. (1996). Queer current and pacemaker: The Hyperpolarization-Activated Cation Current in Neurons. *Annual Reviews Physiology, 58*, 299-327.

Percy, W. H., & Krier, J. (1987). Cholinergic excitatory synaptic potentials of neurones in mammalian lumbar paravertebral ganglia. *J Auton Nerv Syst, 18*(3), 195-205.

Platkiewicz, J., & Brette, R. (2010). A threshold equation for action potential initiation. *PLoS Comput Biol, 6*(7), e1000850. doi:10.1371/journal.pcbi.1000850

Powers, R. K., Sawczuk, A., Musick, J. R., & Binder, M. D. (1999). Multiple mechanisms of spike-frequency adaptation in motoneurones. *The Journal of Physiology, 93*, 101-114.

Rimmer, K., & Horn, J. P. (2010). Weak and straddling secondary nicotinic synapses can drive firing in rat sympathetic neurons and thereby contribute to ganglionic amplification. *Front Neurol, 1*, 130. doi:10.3389/fneur.2010.00130

Rush, M. E., & Rinzel, J. (1995). The potassium A-current, low firing rates and rebound excitation in Hodgkin-Huxley models. *Bulletin of mathematical biology, 57*, 899–929.

Springer, M. G., Kullmann, P. H., & Horn, J. P. (2015). Virtual leak channels modulate firing dynamics and synaptic integration in rat sympathetic neurons: implications for ganglionic transmission *in vivo*. *J Physiol, 593*(4), 803-823. doi:10.1113/jphysiol.2014.284125

Springer, M. G., Kullmann, P. H. M., & Horn, J. P. (2015). Virtual leak channels modulate firing dynamics and synaptic integration in rat sympathetic neurons: implications for ganglionic transmission *in vivo*: Firing dynamics and synaptic gain in rat sympathetic neurons. *The Journal of Physiology, 593*, 803-823. doi:10.1113/jphysiol.2014.284125

Stauffer, E. K., McDonagh, J. C., Hornby, T. G., Reinking, R. M., & Stuart, D. G. (2007). Historical reflections on the afterhyperpolarization–firing rate relation of vertebrate spinal neurons. *J Comp Physiol A Neuroethol Sens Neural Behav Physiol, 193*(2), 145-158. doi:10.1007/s00359-006-0198-2

Steinback, C. D., Salmanpour, A., Breskovic, T., Dujic, Z., & Shoemaker, J. K. (2010). Sympathetic neural activation: an ordered affair. *J Physiol., 588*(Pt 23), 4825-4836. doi: 4810.1113/jphysiol.2010.195941. Epub 192010 Oct 195911.

Undem, B. J., & Potenzieri, C. (2012). Autonomic neural control of intrathoracic airways. *Compr Physiol, 2*(2), 1241-1267. doi:10.1002/cphy.c110032

Wang, F. B., Holst, M. C., & Powley, T. L. (1995). The ratio of pre- to postganglionic neurons and related issues in the autonomic nervous system. *Brain Res Brain Res Rev., 21*(1), 93-115.

Wheeler, D. W., Kullmann, P. H., & Horn, J. P. (2004). Estimating use-dependent synaptic gain in autonomic ganglia by computational simulation and dynamic-clamp analysis. *J Neurophysiol, 92*(5), 2659-2671. doi:10.1152/jn.00470.2004

h. posters

Characterization of cell number and size in T5 paravertebral ganglia following T2 spinal cord transection: Implications for autonomic dysreflexia.

Galvin ML, Sokoloff AJ, Sawchuk M, Hochman S. Emory University, Department of Physiology

INTRODUCTION

Autonomic Dysreflexia (AD) is a potentially life-threatening condition that results from spinal cord injury (SCI) above the T5-6 spinal level. The condition is marked by excessive hypertension due to over-activity of the Autonomic Nervous System. AD is considered a medical emergency requiring immediate attention because persistent elevated hypertension can lead to stroke or death.

AD is initiated by a noxious stimulus arising below the injury level (typically bladder distention, impacted bowel, or bedsores). In a healthy individual physiological circuitry is tuned to respond to pain or discomfort accordingly. However, in SCI patients, ascending sensory signals are blocked at the site of the injury and prevent perception of noxious signaling. Additionally, disruption of descending control of the sympathetic nervous system due to SCI prevents a normal physiological response to decrease hypertension. In this situation noxious afferents have complete control over activation of spinal sympathetic neurons resulting in a large and persistent increase in blood pressure (Figure 1).

Figure 1: Autonomic Dysreflexia

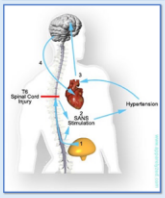

Figure 1: Ascending and Descending signals are blocked at the level of the spina cord injury inhibiting communication between the brain and periphery organs.

Paravertebral Sympathetic Ganglia

How exactly does distention or pain cause hypertension? Animal experiments suggest that SCI leads to sprouting of the pain afferents that project to the sympathetic preganglionic neurons in the spinal cord (Figure 2A, Rabchevsky). It is thought that this amplified sensory input contributes significantly to the exaggerated sympathetic response associated with hypertension.
However it is also possible that the sympathetic post-ganglionic neurons that lie in thoracic chain ganglia and innervate vasculature may also contribute to amplified hypertensive response in AD. This possibility remains uninvestigated.

Figure 2: Pain Afferent Sprouting

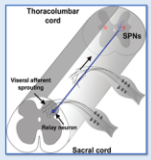

Figure 3: Thoracic Chain Ganglia

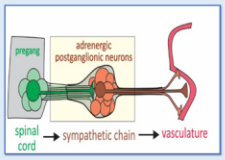

Figure 2: Rabchevsky's group showed that the observed AD after SCI was associated with sprouting of pain afferents and spinal projections to sympathetic autonomic output neurons (Hou et al., 2008).
Figure 3: Principles of input-out vasomotor gain control through thoracic chain ganglia.

It is likely that there are also anatomical and physiological changes in paravertebral postganglionic neurons after SCI. This study tested the hypothesis that high thoracic SCI provokes anatomical changes in thoracic chain ganglia near the injury site. We examined neurons comprising the T5 paravertebral sympathetic ganglia three weeks after SCI.

METHODS AND ANALYSIS

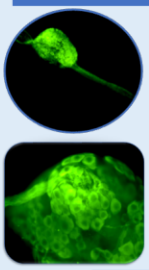

METHODS

- Mouse model: male and female
- Spinal transection at thoracic level two (T2)
- 7 SCI mice; 5 naive control
- Twenty-one day survival
- Harvest of T5 ganglion
- Whole ganglion immunohistochemical reaction for tyrosine hydroxylase (TH)
- Count and size (area/diameter) of T5 neurons positive for TH in Neurolucida software

Table1: Comparison of Cell Area and Diameter

	SCI (N = 7)	Naive (N = 5)	P-Value	Power	Male (N=7)	Female (N=5)	P-Value	Power
Mean Area	297.864*	373.534*	**0.0208**	0.696	344.768	307.869	0.311	0.162
Std. Dev.	25.424	60.597	-	-	307.869	64.604	-	-
Mean Diameter	20.851*	23.510*	**0.0149**	0.753	22.606	21.053	0.201	0.236
Std.Dev.	1.342	1.813	-	-	1.623	2.331	-	-

Figure 5

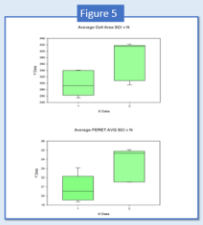

Figure 6

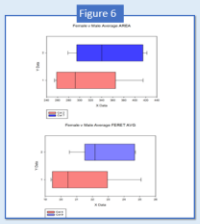

Table 1: Data of T5 paravertebral sympathetic ganglia in spinalized (T2) mice and naive mice. We conducted a T-test with an alpha level of a=0.05 for both average area and average diameter.
Figure 5: Box-Plot of average cell area and diameter in SCI T5 ganglia (N=7) compared to average cell area and diameter in naive T5 ganglia (N=5).
Figure 6: Box-Plot of average cell area and diameter in female T5 ganglia (N=5) as compared to male T5 ganglia (N=7).

Table 2: Average cell count in spinalized versus naive T5 ganglia.

Cell Count/Ganglion	N=	Mean	Standard Dev.	Standard Error
SCI	7	194.429	77.036	29.117
Naive	5	270.600	127.443	56.994

Table 2: Average cell number in SCI T5 ganglia (N=7) compared to average cell number in naive T5 ganglia (N=5). We conducted a T-test with an alpha level of a=0.05 for both average area and average diameter.

RESULTS

Area: The difference in the mean values of the average area for SCI versus naive is greater than would be expected by chance; there is a statistically significant difference between the treatment groups' average cell area (P = 0.0208). At an alpha level of 0.05 we can deduce that this difference in means is statistically significant. However, the power of the performed test (0.696) is below the desired power of 0.800. Less than desired power indicates you are less likely to detect a difference when one actually exists.

Diameter : The difference in the mean values of the diameter for SCI versus naive is greater than would be expected by chance; there is a statistically significant difference between the treatment groups (P = 0.0149). At an alpha level of 0.05 we can deduce that this difference in means is statistically significant. However, the power of the performed test (0.753) is below the desired power of 0.800. Less than desired power indicates you are less likely to detect a difference when one actually exists.

We hypothesized that the statistically significant differences in cell area and diameter between SCI and naive T5 ganglia could be due to influence of sex rather than treatment. However, when we compared the average area and diameter of male versus females we saw no significant differences in mean areas or diameters. Within the constraints of our limited population size, we conclude that sex is not a factor.

DISCUSSION

We hypothesize that, in response to the exaggerated sympathetic response associated with the amplified sensory input may cause postganglionic neurons to undergo compensatory response to reduce their excitability (e.g. pruning of preganglionic synaptic inputs, reduced dendritic arborizations and reduction of cell size).

Further studies would have to control for compounding factors such as sex, left or right ganglia. In addition, we would have to collect more data from more ganglia in order to increase statistical power.

Acknowledgements

I would like to thank Mike Sawchuk, Dr. Alan Sokoloff and Dr. Shawn Hochman and Dr. Leah Roesch for their mentorship and guidance.

References

Hou, S. et al (2008). Plasticity of lumbosacral propriospinal neurons is associated with the development of autonomic dysreflexia after thoracic spinal cord transection. *J Comp Neurol* 509(4), 382-99.
McCorry, LK (2007). Physiology of the autonomic nervous system. *Am. J. Pharm. Edu* 71(4), 78.
McLachlan, EM (2007). Diversity of sympathetic vasoconstrictor pathways and their plasticity after spinal cord injury. *Clin Auton Res* 17:6-12.
Rabchevsky, AG (2006). Segmental organization of spinal reflexes mediating autonomic dysreflexia after spinal cord injury. *Prog Brain Res* 152:265 – 74.
Smolen, AJ (1988). Morphology of synapses in the autonomic nervous system. *J Electron Microsc* 10:187-204.